HHS Public Access

Author manuscript

Immunity. Author manuscript; available in PMC 2016 September 15.

Published in final edited form as:

Immunity. 2015 September 15; 43(3): 463–474. doi:10.1016/j.immuni.2015.07.022.

Cytosolic nuclease TREX1 regulates oligosaccharyltransferase activity independent of nuclease activity to suppress immune activation

Maroof Hasan[1,2,@,*], **Charles S. Fermaintt**[1,2,*], **Ningguo Gao**[3,#], **Tomomi Sakai**[4], **Takuya Miyazaki**[4,&], **Sixin Jiang**[3,%], **Quan-Zhen Li**[5], **John P. Atkinson**[6], **Herbert C. Morse III**[4,§], **Mark A. Lehrman**[3,§], and **Nan Yan**[1,2,§]

[1]Department of Internal Medicine, University of Texas Southwestern Medical Center, Dallas, Texas, 75390, USA

[2]Department of Microbiology, University of Texas Southwestern Medical Center, Dallas, Texas, 75390, USA

[3]Department of Pharmacology, University of Texas Southwestern Medical Center, Dallas, Texas, 75390, USA

[5]Department of Immunology, University of Texas Southwestern Medical Center, Dallas, Texas, 75390, USA

[4]Virology and Cellular Immunology Section, Laboratory of Immunogenetics, National Institute of Allergy and Infectious Diseases, National Institutes of Health, Rockville, Maryland, 20852, USA

[6]Department of Medicine, Division of Rheumatology, Washington University School of Medicine, St. Louis, Missouri, 63110, USA

Abstract

TREX1 is an endoplasmic reticulum (ER)-associated negative regulator of innate immunity. TREX1 mutations are associated with autoimmune and autoinflammatory diseases. Biallelic mutations abrogating DNase activity cause autoimmunity by allowing immunogenic self-DNA to accumulate, but it is unknown how dominant frame-shift (fs) mutations that encode DNase-active but mislocalized proteins cause disease. We found the TREX1 C-terminus suppressed immune

Correspondence to: N.Y. (nan.yan@utsouthwestern.edu). M.A.L (mark.lehrman@utsouthwestern.edu).
*Co-first author.
§Co-senior author.
@Present address: Novartis Institutes for BioMedical Research, CH-4056 Basel, Switzerland.
#Present address: Xbiotech, Austin, TX, 78744, USA.
&Present address: Department of Internal Medicine and Clinical Immunology, Yokohama City University Graduate School of Medicine, Yokohama, 236-0004, Japan.
%Present address: Albany Medical College, Albany, NY, 12208, USA.

Author contributions:
M.H., C.F., N.G., S.J. and N.Y. performed experiments and data analyses with input from H.C.M. and M.A.L. T.S., T.M. and H.C.M. generated the TREX1-V235fs mice and helped to characterize the mice. Q.Z.L. helped autoantibody array experiments. J.P.A generated the TREX1 antibody and RVCL lymphoblast cell lines. M.H., J.P.A., H.C.M., M.A.L. and N.Y. wrote the paper.

activation by interacting with the ER oligosaccharyltransferase (OST) complex and stabilizing its catalytic integrity. C-terminal truncation of TREX1 by fs mutations dysregulated the OST complex, leading to free glycan release from dolichol carriers, as well as immune activation and autoantibody production. A connection between OST dysregulation and immune disorders was demonstrated in Trex1$^{-/-}$ mice, TREX1-V235fs patient lymphoblasts, and TREX1-V235fs knock-in mice. Inhibiting OST with aclacinomycin corrects the glycan and immune defects associated with Trex1-deficiency or fs mutation. This function of the TREX1 C-terminus suggests a potential therapeutic option for TREX1-fs mutant-associated diseases.

Graphical Abstract

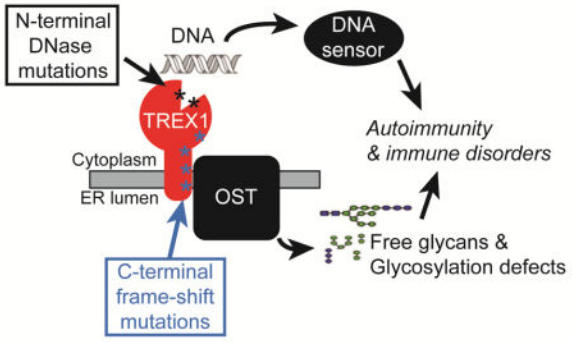

INTRODUCTION

Mammalian cells have evolved negative regulators of innate immunity to protect against autoimmune activation. These negative regulators either remove immunogenic self-ligands accumulated in the wrong place (e.g. self-DNA in the cytosol) (Holm et al., 2013), or act upstream to prevent production of self-ligands or their precursors (e.g. erroneous lipids or glycans with abnormal branching) (Green et al., 2007; Kawasaki et al., 2013). We have focused on the negative regulator TREX1 (DNase III), a 3′→5′ exonuclease (Hasan et al., 2013; Yan et al., 2010). As a single locus, TREX1 mutations are associated with a surprisingly broad spectrum of autoimmune and inflammatory phenotypes, including Aicardi-Goutières syndrome (AGS), familial chilblain lupus (FCL), systemic lupus erythematosus (SLE) and retinal vasculopathy with cerebral leukodystrophy (RVCL) (Crow and Rehwinkel, 2009). TREX1 protein has an exonuclease domain at the N-terminus and an ER localization domain at the C-terminus, containing a single-pass transmembrane (TM) motif tail-anchoring TREX1 on the ER (Lee-Kirsch et al., 2007; Lindahl et al., 2009). Recessive missense mutations in the TREX1 DNase domain (e.g. D18N and D200N (Fye et al., 2011; Lehtinen et al., 2008)) are predominantly associated with AGS, an early onset autoimmune disease with severe clinical presentation. In contrast, dominant frame-shift mutations that truncate the C-terminus remain DNase-active (e.g. V235fs and D272fs (de Silva et al., 2007; Lee-Kirsch et al., 2007; Richards et al., 2007)) and largely associate with RVCL (and in some cases SLE) with later onset and less severe disease (see summary diagram in Figure S1A) (Crow and Rehwinkel, 2009; Richards et al., 2007). In AGS the diminished TREX1 DNase activity leads to accumulation of self-DNA from replication debris (Yang et al., 2007) or endogenous retroelements (Stetson et al., 2008), likely

contributing to sterile inflammation. However, such etiology does not explain disease caused by C-terminal frame-shift mutations. Here, we report an unexpected new function of the TREX1 C-terminus for maintaining catalytic fastidiousness of the ER enzyme complex oligosaccharyltransferase (OST). OST dysregulation caused by TREX1 C-terminal truncation leads to hydrolytic release of free glycans from dolichol (lipid)-linked oligosaccharides (LLO), as well as immune activation and autoantibody production. The identification of distinct functions of the TREX1 N-terminal and C-terminal regions, with connection between OST and immune disorders in the latter case, provides a biochemical framework for understanding the two classes of TREX1 diseases and more specifically the effects of RVCL frame-shift truncations.

RESULTS

TREX1 C-terminus plays a critical role in suppressing immune activation

We reported that Trex1-deficiency causes cell-intrinsic activation of immune genes (e.g. IFN-stimulated genes or ISGs) in an IFN-independent manner (Hasan et al., 2013), but the roles of the C-terminal ER localization domain in activation of immune genes were unclear. Thus, we examined lymphoblasts from six unrelated RVCL patients carrying the dominant TREX1-V235fs mutation and three healthy controls with normal TREX1. All RVCL patient cells had elevated ISG transcripts (e.g. CXCL10 mRNA, Figure 1A). Since TREX1-V235fs is dominant, we confirmed the dual expressions of normal and C-terminal truncated TREX1 in RVCL patient cells with a new antibody against the TREX1 N-terminus (Figure 1B). The truncated TREX1 protein is DNase active but mislocalized throughout the cell (Richards et al., 2007). We also found that human lymphoblasts are devoid of components of cytosolic DNA sensing pathway such as cGAS and STING, and that lymphoblasts activate IFN expression in response to RNA, but not DNA, stimulation (Figure S1B, S1C). These data suggested that the TREX1 C-terminus (perhaps involving ER localization) had a key role in suppressing cell-intrinsic immune gene activation, independent of DNA sensing.

To examine the function of TREX1's C-terminus, we reconstituted mouse Trex1$^{-/-}$ fibroblasts (MEFs) with normal human TREX1 (KO-TREX1) that localizes to the ER, a C-terminal truncation (KO-TREX1_TM) that localizes throughout the cell, a chimera that mislocalizes the truncated TREX1 to the nucleus (KO-TREX1_TM-nls), TREX1's C-terminus fused to GFP that localizes to the ER (GFP-TM), or GFP alone (KO-GFP) (Figure 1C, 1D). Normal TREX1 strongly suppressed Ifit1 mRNA expression and overall ISG signature induction in Trex1$^{-/-}$ cells. In contrast, TREX1_TM only partially suppressed ISG expression (Figure 1E–1G), and the residual rescuing activity was likely contributed from the active DNase domain mislocalized in the cytoplasm. Consistent with this, TREX1_TM-nls, which localizes to the nucleus, has only marginal activity in suppressing ISG expression (Figure 1E–1G). We confirmed that TREX1ΔTM is DNase active on both ssDNA and dsDNA substrates in vitro and in-cell (Figure S1D–G). Conversely, GFP-TM that localized to the ER reduced ISGs by 3–5-fold (Figure 1E–1G), suggesting that TREX1 C-terminus is functional by itself (without the DNase domain) for suppressing ISG induction, and that both N-terminal DNase domain and C-terminal ER localization domain are required for fully suppressing ISG activation in Trex1$^{-/-}$ MEFs. Collectively, our data with RVCL

patient cells and Trex1$^{-/-}$ rescue MEFs suggest that the TREX1 C-terminus is critical for suppressing cell-intrinsic immune activation, with a yet to be identified role in ER biology that may be the underlying cause of RVCL.

OST activity is dysregulated in *Trex1*$^{-/-}$ cells

A major function of the ER is asparagine-linked (N-linked) glycosylation of nascent polypeptides. This involves biosynthesis of the 14-sugar glycan glucose$_3$mannose$_9$N-acetylglucosamine$_2$ ($G_3M_9Gn_2$) linked to the polyisoprene lipid dolichol by a labile pyrophosphate bond, i.e. a lipid-linked oligosaccharide (LLO). The ER enzyme OST transfers the $G_3M_9Gn_2$ glycan to asparaginyl residues in the context Asn-X-Ser/Thr of nascent proteins. However, under conditions such as ER stress (Gao et al., 2011), viral infection (Gao et al., 2011), or hereditary metabolic error (Cline et al., 2012), LLO hydrolysis can be stimulated and free glycans liberated from LLOs begin to accumulate in the ER lumen (Figure S2A). The free glycans are processed to smaller fragments that potentially span the entire luminal space from ER to Golgi, endosomes, and lysosomes (Gao et al., 2011). Aberrant mammalian glycans can be immunogenic and cause autoimmune phenotypes as in α-mannosidase II-deficiency (Chui et al., 2001; Green et al., 2007).

To explore potential links between TREX1 and ER glycan metabolism, we used fluorophore-assisted carbohydrate electrophoresis (FACE) (Gao and Lehrman, 2006), a quantitative technique for assessment of steady-state concentrations of a variety of cellular saccharides. Surprisingly, Trex1$^{-/-}$ MEFs contain 6-fold more total free glycans in vesicular compartments (defined by cell association after selective plasma membrane permeabilization with streptolysin-O (SLO)) compared to wild type cells (Figure 2A), with a ~40% reduction of $G_3M_9Gn_2$-LLO (the precursors of free glycans) (Figure S2B). Steady-state LLO measurements are not expected to decrease to the same extent as the increase observed for free glycans, because LLOs are continuously resynthesized while free glycans accumulate. With an “in-cell” assay, we showed directly that free glycan formation by LLO hydrolysis was accelerated in Trex1$^{-/-}$ MEFs, indicating OST dysfunction (Figure S2C). However, in Trex1$^{-/-}$ cells we did not observe gross qualitative or quantitative changes in total cellular N- or O-linked glycans (Figure S2D, S2E). Free glycan accumulation in Trex1$^{-/-}$ cells appeared independent of ER stress, since Trex1$^{-/-}$ cells lacked a strong ER stress response, although Trex1$^{-/-}$ cells may be more sensitive to exogenous ER stressors (Figure S2F–J).

Like MEFs, Trex1$^{-/-}$ bone marrow-derived macrophages (BMDM), heart, and kidney all contained more free glycans compared to WT (Figure 2B, Figure S2K, S2L). We also detected more free glycans in Trex1$^{-/-}$ mouse serum compared to WT (Figure 2B, Figure S2L), consistent with secretion. Since they bind to Con A efficiently, Trex1$^{-/-}$ MEF free glycans are likely high-mannose, hybrid, or biantennary-complex type (Figure S2N).

Since ER localization of TREX1 is required for suppressing the ISG signature (Figure 1), we examined its role in controlling free glycan production by FACE analysis of rescued Trex1$^{-/-}$ MEFs (Figure 2C). While WT TREX1 strongly suppressed free glycan accumulation in Trex1$^{-/-}$ cells, mislocalized but DNase-active TREX1_TM and TREX1_TM-nls failed to appreciably reduce free glycans levels. Equally important, DNase-

inactive TREX1-D18N that was properly ER-localized diminished free glycan concentrations to those of WT and TREX1 rescue cells, showing that DNase activity is dispensable for TREX1 to suppress free glycan accumulation. Thus, the TREX1 C-terminus has an unexpected DNase-independent function associated with ER glycan metabolism.

Products of OST dysregulation are immunogenic

We next asked whether Trex1$^{-/-}$ free glycans might contribute to immune activation. Free glycan pools from WT and Trex1$^{-/-}$ cells were incubated with wild type BMDMs, then expression of immune and housekeeping genes was measured with a qPCR array. Free glycan pools from Trex1$^{-/-}$ cells, but not from WT cells, induced strong expression (5–20 fold increase) of many ISGs in wild type BMDMs (Fig. 3A), but not housekeeping, IFN, and inflammatory genes, similar to the ISG signatures of Trex1$^{-/-}$ and RVCL patient cells (Figure 1). We also treated the free glycan pool with a combination of DNase, RNase and proteases or eluted them from FACE gels to eliminate contamination concerns. The treated and gel purified glycan pool was still able to induce ISGs in wild type BMDMs (Figure 3A, 3B). In contrast, $Man_{5\text{-}9}GlcNAc_2$ high-mannose N-glycan mixtures from RNase B after PNGase treatment (consisting of at least 5 discrete species by FACE) did not stimulate ISGs when added to macrophages (Figure 3C). This suggests that bioactive Trex1$^{-/-}$ free glycans are not typical high-mannose containing structures, perhaps glucosylated or paucimannose instead. Indeed, we found that Trex1$^{-/-}$ free glycan pools contain smaller differing structures compared to RNaseB N-glycan (Figure 3C). Using BMDMs derived from specific knockout mice, we also determined that free glycan-induced immune activation is TBK1-dependent, but cGAS-STING-independent (Figure S3A–D). We note that in these experiments free glycans were added exogenously, which may lead to activation of immune pathways that are different from pathways that might be activated when glycan pools are derived endogenously in Trex1$^{-/-}$ cells. Nevertheless, these data suggest that free glycans have the potential to induce the ISG signature commonly associated with TREX1 diseases.

TREX1 helps OST act as a peptide-dependent transferase rather than a hydrolase

Converting LLOs to free glycans should lead to less donor substrate available for N-glycosylation and loss of glycan shielding of potentially antigenic sequences. To test this possibility, we performed the ‘In-cell’ OST activity assay (a diagram in Figure S3E). WT and Trex1$^{-/-}$ MEFs were permeabilized by SLO and incubated with reaction buffer containing nucleotide sugars for LLO synthesis and control or acceptor peptide. Only the acceptor peptide contains a N-glycosylation site. Both transferred N-glycans (cleaved with EndoH) and free glyans (from LLO hydrolysis) were analyzed by FACE. In WT cells, transferred N-glycans increased and free glycans decreased with acceptor peptide present, consistent with the fact that both transfer and hydrolysis activities of OST utilize the same pool of incoming substrate (LLOs in the ER membrane, as shown in Figure S3E). We then compared each OST activity in WT versus Trex1$^{-/-}$ cells. While OST hydrolysis activity was elevated by 2-fold, acceptor peptide appeared underglycosylated in Trex1$^{-/-}$ compared to WT cells by 2-fold (Figure 3D). This suggests that OST transfer activity for N-glycosylation may be limiting in permeabilized Trex1$^{-/-}$ cells, either due to insufficient LLO, or a kinetic difference in the absence of TREX1. Thus, OST is enzymatically active in Trex1$^{-/-}$ cells, but its preference for peptide targets versus water may be compromised. We

next tried to detect glycosylation defects in endogenous proteins. However, glycosylation analysis with live cells (Western blot analysis of several endogenous glycoproteins or measurement of total N-linked glycans) failed to reveal a significant glycosylation defect in Trex1$^{-/-}$ cells or RVCL patients lymphoblasts compared to WT or healthy control cells, respectively (data not shown). Collectively, these data suggest that Trex1-deficiency has the potential to cause N-glycosylation defects, likely affecting proteins with less favorable acceptor sequons such that a small subset of glycoproteins would be primarily affected.

TREX1 interacts with the OST complex on the ER through the C-terminus

Since the absence of TREX1 accelerated LLO hydrolysis by OST, we asked whether the two enzymes interacted physically. The mammalian OST complex contains 7–8 subunits, with two alternative catalytic subunits (STT3A and STT3B) (Kelleher and Gilmore, 2006). We co-expressed TREX1-V5 and various Myc-tagged OST subunits in 293T cells, and assessed interactions by immunoprecipitation (IP). We found strong interactions between TREX1 and two subunits, DDOST and RPN1, but failed to detect interaction with two other subunits, RPN2 and STT3A (Figure 4A). Immunprecipitation of OST subunits was completely dependent upon the presence of TREX1 (Figure 4B). We validated TREX1:RPN1 and TREX1:DDOST interactions by reverse IPs (Figure 4C). Notably, C-terminal truncation of TREX1 (TREX1_TM) drastically reduced the interaction with RPN1, consistent with OST interacting with TREX1 through its C-terminus (Figure 4D). Immunofluorescence microcopy revealed extensive colocalization of TREX1 and RPN1 at the ER (Figure 4E).

These data led us to hypothesize that OST might signal the absence or dissociation of TREX1 from the ER, and be involved in ISG induction in Trex1$^{-/-}$ cells. Upon depletion of individual OST subunits in Trex1$^{-/-}$ cells with specific shRNAs, we found that Rpn1 and Stt3a depletion both suppressed Ifit1 mRNA expression while Rpn2 and Stt3b depletion did not (Figure 4F, Figure S4). These results implicate OST itself in suppressing cell-intrinsic immune activation caused by disruption of Trex1. In conjunction with our co-IP studies, we infer that while RPN1 interacts physically with TREX1, STT3A (one of the two catalytic subunits of OST) appears to control ISGs without an interaction with TREX1 detectable by co-IP.

Inhibiting OST activity by aclacinomycin corrects glycan and immune defects in *TREX1* mutant cells

To better link OST activity with immune disorders, and to explore this interaction as a therapeutic target, we tested a small pharmacologically-active molecule, aclacinomycin A (Acm) (Bennett et al., 2013). Acm is FDA-approved for treating acute myeloid leukemia (Majima and Ohta, 1987), and was previously implicated in impairing OST function. However, the precise mechanism was unclear (Bennett et al., 2013; Morin and Sartorelli, 1984). Here, we performed the in-cell OST activity assay (Figure 3D) in permeabilized WT or Trex1$^{-/-}$ MEFs treated with DMSO or Acm. We found that Acm inhibited both known activities of OST: transfer of glycan to asparaginyl acceptors; and LLO hydrolysis yielding free glycans (Figure 5A, Figure S5A–E). With live Trex1$^{-/-}$ cells we then found that both LLO hydrolysis and ISG activation were diminished in parallel after 24 h of Acm treatment (Figure 5B, 5C). Acm treatment also reduced the lysosomal gene signature in Trex1$^{-/-}$ cells

(Figure S5F), consistent with a glycosylation defect acting upstream of the lysosome expansion phenotype that we observed previously (Hasan et al., 2013). To test Acm in vivo, we treated Trex1$^{+/-}$ and Trex1$^{-/-}$ mice with DMSO or Acm for 8 weeks. Trex1$^{-/-}$ mice usually show splenomegaly and discoloration of the liver due to systemic inflammation and autoimmunity, as well as elevated ISGs especially in the heart (Gall et al., 2012; Hasan et al., 2013). Acm treatment in vivo significantly reduced the ISG signature in Trex1$^{-/-}$ mouse heart and spleen, and improved both spleen and liver phenotypes (Figure 5D, 5E). Importantly, Acm significantly improved survival of Trex1$^{-/-}$ mice (Fig 5F). Collectively, our data suggest that OST dysregulation is an important contributing factor for TREX1 disease and that inhibiting OST with Acm may be an efficacious therapeutic option.

To further validate the therapeutic potential of Acm to treat TREX1 frame-shift patients, we examined OST dysfunction in lymphoblasts from TREX1 V235fs (RVCL) patients and healthy controls. All RVCL patient cells had elevated amounts of free glycan (Figure 6A, 6B) compared to healthy controls. Importantly, all RVCL patient cells responded to Acm treatment, which restored free glycan and CXCL10 mRNA levels to normal (Figure 6C, 6D).

TREX1-V235fs knock-in mouse display elevated immune gene signature, free glycans and autoantibodies

To better model human RVCL disease, we generated TREX1-V235fs knock-in mice (‘RVCL mouse’, Figure S6A). We confirmed the expression of a human TREX1-V235fs truncation and loss of mouse Trex1 expression in BMDMs of the RVCL mouse (Figure 7A). Both heterozygous and homozygous TREX1-V235fs mice are grossly normal, and without inflammation detected in any tissue (data not shown). This suggests that RVCL mice do not suffer from self-DNA mediated systemic inflammation, consistent with clinical findings of RVCL patients and with mislocalized V235fs DNase being functional. Yet, RVCL mouse BMDMs express elevated ISGs compared to WT littermates (Figure 7B), with a 3-fold increase in free glycans (Figure 7C). We detected strong autoantibody production in RVCL mouse serum against a spectrum of disease-associated protein antigens (Figure 7D, 7E). Taken together, TREX1 frame-shift mutation cause OST dysregulation and immune disorders, but not DNA-associated systemic inflammation in vivo. Whether RVCL mice develop vision and neurological symptoms as in human patients awaits further investigation. Trex1$^{-/-}$ mice have been very useful in studying human TREX1 diseases, although they do not distinguish different diseases associated with TREX1 mutations affecting the DNase domain or the C-terminus. The RVCL knock-in mouse presented here is thus a better model for studying diseases associated with TREX1 C-terminal frame-shift mutations, and will allow testing of different hypotheses for OST dysregulation leading to immune disorders.

DISCUSSION

The discordance between the genetics and clinical etiologies of AGS versus RVCL predicted a novel function of TREX1 associated with the C-terminus, and independent of DNase activity. By focusing on RVCL mutations, we found that truncation of the TREX1 C-terminus dysregulates OST, which like TREX1 is also ER localized. This finding suggests

that mutations disrupting different parts of TREX1 can cause clinically distinct phenotypes. We propose that TREX1 AGS (recessive) is caused by self-DNA sensing when both copies of the DNase domain are defective, consistent with a requirement for a catalytic function and severe clinical diseases in childhood. In contrast, TREX1 RVCL (dominant) is likely caused by OST dysregulation when one copy of TREX1 loses the C-terminus, disrupting its interaction with the OST complex and leading to a plethora of downstream effects. This is consistent with a slower progression of RVCL disease, with typical onset in adulthood to older age (Richards et al., 2007) Moreover, we found that RVCL patient cells had strong induction of ISGs including CXCL10 mRNA. Since CXCL10 inhibits angiogenesis (Taylor et al., 2008), and induces dissociation of newly formed blood vessels (Bodnar et al., 2009), elevated CXCL10 could be a major contributor to systemic vasculopathy in RVCL patients.

How might OST dysregulation lead to such immune phenotypes in RVCL? For C-terminal truncations of TREX1 typical of RVCL alleles, we identified two robust biochemical effects on glycan metabolism. First, dysregulated OST hydrolyzes LLOs at an abnormal rate. This reduces the steady-state concentrations of LLOs needed for N-linked glycosylation. Within our limits of sensitivity, we detected no global defects in total N-linked glycosylation in $Trex1^{-/-}$ cells. However, underglycosylation of a small subset of glycoproteins with unfavorable glycosylation acceptor sequences (sequons) remains possible. Over an extended period, the absence of “glycan shielding” could lead to immune responses to bare epitopes that would induce production of novel autoantibodies. Second, accelerated LLO hydrolysis increased release of free glycans. These “self” glycans could, for example, mimic surface glycans of certain pathogens that can be recognized by lectin receptors on macrophages and dendritic cells to activate immune responses. And we found that free glycan pools isolated from $Trex1^{-/-}$ cells do have immunogenic potential, although the exact immune pathway and glycan structure(s) being recognized require further investigation. The ability of OST subunit knockdown and inhibitor Acm to block both free glycan release and ISG induction also supports the immunogenic “self” glycan hypothesis. Third, the same free glycans in the ER lumen could compete with nascent immunomodulatory surface proteins for binding to chaperone-lectins and enzyme-lectins in the secretory pathway to impair their folding or quality control, or compete with downstream glycan modifying processes and ultimately interfere with formation of galectin-stabilized cell surface lattices that may enhance signaling. As a general precedent for these ideas, defects in the glycan modifying enzyme α-mannosidase II abnormally increased hybrid N-glycans that are potential ligands for mannose-binding lectin receptors, and caused SLE-like phenotypes in mice (Chui et al., 2001; Green et al., 2007). These various hypotheses for OST dysfunction leading to immune disorders should not be mutually exclusive, and while testing these ideas experimentally is beyond the scope of the present study, our new TREX1-V235fs knock-in mouse model will be very useful for further elucidating the exact nature of glycan or glycosylation defects caused by TREX1 frame-shift mutations, and how they induce immune activation and autoantibody production.

A recently published TREX1-D18N knock-in mouse showed DNA-mediated systemic inflammation and lupus-like syndrome similar to $Trex1^{-/-}$ mice, although with much longer survival (>40 weeks) comparing to $Trex1^{-/-}$ mice (8–10 weeks) (Grieves et al., 2015). These observations suggest that both DNA- and glycan-mediated immune defects contribute

to severe disease in Trex1$^{-/-}$ mice. These two new knock-in mouse models (D18N and V235fs) focusing on distinct functions of TREX1 will be incredibly useful tools for further understanding TREX1 biology.

Despite extensive understanding of the composition of the OST complex and its enzymatic activity, and numerous examples of glycan-lectin interactions in the immune system, OST itself has never been directly connected to an immune disorder, and the immune consequences of OST dysregulation have therefore been unexplored. Thus, our findings will be very useful in revealing OST's role in immunoglycobiology, including inhibition of OST with Acm or similar compounds for treating TREX1 C-terminal frame-shift diseases.

Methods

Cells, viruses and mice

Trex1$^{+/-}$ mice were provided by D. Stetson (U. Washington) under an agreement with D. Barnes and T. Lindahl (Cancer Research UK)(Morita et al., 2004). WT, P212fs and D18N human skin fibroblasts were kindly provided by M-A. Lee-Kirsch (TU Dreston, Germany). HeLa and 293T cells have been described(Yan et al., 2010). These cells were maintained in Dulbecco's modified Eagle's medium (DMEM) with 10% (v/v) heat-inactivated fetal calf serum (FCS), 2 mM L-glutamine, 10 mM HEPES and 1 mM sodium pyruvate (complete DMEM) with the addition of 100 U/ml penicillin, 100 mg/ml streptomycin and cultured at 37°C with 5% CO2. EBV-transformed lymphoblasts from healthy controls and TREX1 RVCL patients were maintained in RPMI with the same 10% FCS and supplements. Bone marrow-derived macrophages were generated as described (Hasan et al., 2013). VSV-GFP (Das et al., 2006) were provided by A. K. Pattnaik (U. Nebraska). Cells were infected with the indicated virus, MOI and time points and washed three times with 1X PBS before subsequent analysis. For Trex1$^{-/-}$ MEFs reconstituted with various TREX1 rescuing constructs, WT or mutant or truncated TREX1 was cloned into retroviral MRX-ibsr vector (Saitoh et al., 2009) (a kind gift from S. Akira) using Eco RI and Not I sites. Retroviruses were packaged in 293T cells and used for infection of Trex1$^{-/-}$ MEFs followed by selection with blasticidine (Sigma). For shRNA knockdowns, Trex1$^{-/-}$ MEFs were transduced with lentiviruses expressing specific shRNA (pLKO system, Addgene) and selected with puromycin. DNA oligos used for constructing shRNA plasmids are shown in Supplementary Table 1. In vivo experiments with Acm were done by i.p. injections three times per week for 10 weeks. Stocks of DMSO and Acm were further diluted in PBS to obtain 100 microliter total volume per injection for each mouse. Some mouse tissues were harvested on day 7 after treatment for RNA and disease phenotype analysis. Experiments carried out in BSL2 conditions were approved by the Environmental Health & Safety Committee at UT Southwestern Medical Center. Experiments involving human and mouse materials were approved by the ICUAC and IRB of UT Southwestern Medical Center, the Washington University School of Medicine and NIAID (LIP16).

Generation of mice expressing V235fs mutant human TREX1

These mice were generated by Ozgene Pty. Ltd. (Bentley WA) using a C57BL/6 targeting strategy as part of a contract with NIAID, NIH. Conditional humanization of the mouse

Trex1 coding exon was performed by floxing exon 2 and knocking in a human cDNA bearing the V235fs mutation followed by a PGK-Neo cassette. The human cDNA was fused to the UTR sequence from exon 2 and its splice acceptor site and positioned downstream of the Neo cassette in the targeted locus. The PGK-Neo cassette was flanked by FRT sites and was deleted using FLPe recombinase. The gene product containing the human cDNA was expressed after Cre-mediated deletion of mouse exon 2. Mice genotyping was performed using the following primers. *CKI_LoxP primers*, CKI_LoxP_3b (5′-CAGCTCAGCCCTTCCCTTCAGCAG-3′) and CKI_LoxP_5b (5′-ACCCTGCCCTCCAGCTTCTAGTGG-3′). The use of mice in this study followed a protocol (LIG-16E) approved by the National Institute of Allergy and Infectious Diseases Animal Care and Use Committee.

Reagents and antibodies

TRI Reagent (Invitrogen) was used for RNA isolation. Lipofectamine 2000 (Invitrogen) was used for nucleic acid transfections. Aclacinomycin A was purchased from Santa Cruz (sc-200160). Antibodies used in this study include: anti-TREX1 (raised against the N terminus, generated in-house, rabbit, 1:2000), anti-STING (rabbit; 1:1,000 dilution; D2P2F; Cell Signaling), anti-TBK1 (rabbit; 1:1,000 dilution; D1B4; Cell Signaling), anti-cGas (MB21D1) (rabbit; 1:200 dilution; HPA031700; Sigma), anti-Tubulin (mouse; 1:2,000 dilution; B-5-1-2; Sigma), anti-HMGB1 (rabbit; 1:2,000 dilution; ab18256; Abcam), anti-GRP78 (rabbit; 1:1,000 dilution; ab21685; Abcam), anti-V5 (mouse; 1:5,000 dilution; R-960-25; Life Technologies), anti-Myc (rabbit; 1:2,000 dilution; sc-40 ac; Santa Cruz), anti-TREX1 antibody (mouse; 1:200 dilution; sc-271870; Santa Cruz), secondary antibodies (1:4,000 dilution; GE Healthcare) were used for immunoblot analysis according to standard protocols.

qRT-PCR analysis, qPCR array, fluorescence microscopy and FACS

RNA isolation and qRT-PCR analysis were performed as described previously(Hasan et al., 2013). Oligonucleotides are listed in Supplementary Table 1. qPCR array analyses of immune gene profiles were performed using custom ordered PCR array plates containing primer sets pre-aliquoted (Bio-Rad). Each primer set was validated by Bio-Rad and in house. For microscopy, cells grown on coverslips were fixed in 4% (wt/vol) paraformaldehyde and were permeabilized and stained by standard protocols. Samples mounted in Vectashield mounting medium containing DAPI (4,6-diamidino-2-phenylindole; Vector Laboratories) were imaged with a Zeiss Imager M2 fluorescence microscope equipped with AxioVision software. The following antibodies were used for immunostaining: anti-calreticulin (Abcam, Ab4-100), anti-FLAG (Sigma, F1804), anti-V5 (Invitrogen, R960-25), anti-Tubulin (Sigma, B-5-1-2), with Alexa Fluor 488 and 546 tagged secondary antibodies (Invitrogen, A21202, A21206, A10036 and A10040).

Fluorophore-assisted carbohydrate electrophoresis (FACE)

FACE analysis was used to assess total N- and O-linked glycans, LLOs, and free glycans. Cultured cells and snap-frozen mouse tissues were disrupted in methanol, and the resulting suspensions were processed for FACE analyses as described (Gao and Lehrman, 2006). A

three-phase extraction process yielded an aqueous phase containing neutral free glycans (purified further by deionization) and an interfacial layer which was extracted with chloroform:methanol:water (10:10:3) to separate soluble LLOs (which were subsequently depleted of neutral saccharides by ion-exchange chromatography) from insoluble N-linked and O-linked glycoproteins. The glycan units of LLOs were released with weak acid, the N-glycans were released with peptide:N-glycosidase F (C. meningosepticum, Prozyme) or Endoglycosidase H (S. picatus, New England Biolabs), the O-glycans were released with base and sialic acids removed with weak acid, and all three glycan fractions were further purified with ion-exchange resins. All glycans were conjugated with 7-amino-1,3-naphthalenedisulfonic acid (ANDS) and resolved on an oligosaccharide profiling gel, with all loads normalized either to total protein in the chloroform:methanol:water (10:10:3) insoluble residue or total cell number. Glucose oligomers (with four to seven glucosyl residues) and known LLO glycans were also loaded as standards. Fluorescently labeled oligosaccharides were detected with either a Biorad Fluor-S scanner and quantified with Quantity-One software, or a UVP Chemidoc-ItII scanner and quantified with VisionWorks software or ImageJ software.

In-cell OST activity assay

SLO cells permeabilization was performed as described in[15]. Briefly, Trex1$^{-/-}$ and WT MEFs were grown to 80–90% confluency on 0.1% gelatin coated plates to prevent loss of cells thorough the permeabilization process. Cells were subsequently washed with cold PBS twice and later incubated for 5 min with SLO (2 U/ml) on ice. Cells were then washed twice with cold PBS and incubated for 5 min in and 50 mM K-HEPES pH 7.2) at 37 °C followed by a 10 min transport buffer (78 mM KCl, 4 mM $MgCl_2$ incubation on ice in the same buffer to allow for the cytosolic content to diffuse out. Cells were next incubated for 60 min in the reaction buffer (400 uM UDP-Glc, 200 uM UDP-GlcNAc, 50 uM GDP-Man, 2 mM AMP, 10 ug/ml castanospermine and 40 ug/ml deoxymannojirimycin in transport buffer) with either 50 uM of control peptide or acceptor peptide and with or without Aclacinomycin A. After the incubation, cells were washed twice with cold PBS and disrupted by addition of methanol for further FACE analysis.

Co-immunoprecipitation

Approximately 2×10^6 293T were transfected with wild type or mutant TREX1-V5 plasmids and c-Myc OST subnits (STT3A, DDOST, RPN1 or RPN2). Cells were subsequently collected, washed once with PBS, lysed in IP lysis buffer (20 mM Tris-HCl pH 7.4, 150 mM NaCl, 0.5% NP-40 and 1x protease inhibitor mixture) and centrifuged at 20,000g for 20 min at 4°C. The supernatants were mixed with primary antibody and Dynabeads Protein G (Life Technology) and incubated overnight at 4°C. The fallowing day, the beads were washed once with IP buffer, then, twice with high salt IP buffer (500mM NaCl) and finally once with low salt IP buffer (50mM). Immunocomplexes were eluted in 3x Sample buffer and boiled at 95°C for 10 min. Samples were analyzed by immunoblotting.

Exonuclease activity assay

Exonuclease activity assay was performed as described in (Gehrke et al., 2013). Briefly, approximately 1×10^6 293T were transfected with wild type or mutant TREX1-V5 plasmids.

The post-nuclear supernatant isolated as described above, was mixed with anti-V5 agarose beads (Bethyl) and incubated overnight at 4°C. The next day the beads were washed twice with IP buffer and twice with low salt IP buffer. Washed beads were resuspended in 50 ul of DNase buffer (20 mM Tris-HCl (pH 7.5), 5 mM $MgCl_2$, 2 mM DTT, 100 ug/ml BSA and 0.5% NP-40). Either, ssDNA oligo (30-mer) or dsDNA (annealed 30-mer with 3′ overhang resembling cleavage by KpnI, oligo sequence in Supplementary Table 1) were allowed to intercalate SYBR Green II or SYBR Green I respectively (Life Technologies) for 30 min at 37°C in DNase reaction buffer (20 mM Tris-HCl pH 7.4, 5 mM $MgCl_2$, 2 mM DTT, 100 ug/ml BSA, 1/1200 SYBR Green and 10 ng/ul DNA). A volume of 15ul of TREX1 bound beads was mixed with 90 ul of DNase reaction buffer fallowed by real time quantification of DNA/SYBR using a Synergy™HT microplate reader (Biotek) done in triplicates. Beads were later collected for detection of TREX1 expression by immunoblot analysis.

Statistical methods

Data are presented as the mean ± SEM. Graphpad Prism 6 was used for statistical analysis. Statistical tests performed were indicated in figure legend. *P < 0.05, **P < 0.01, ***P < 0.001, and ****P < 0.0001.

Supplementary Material

Refer to Web version on PubMed Central for supplementary material.

Acknowledgments

We thank Min-Ae Lee-Kirsch (TU Dreston, Germany) for TREX1 patient cells; Zhijian ‘James’ Chen for cGAS$^{-/-}$ mice, Russell Vance (UC Berkley) for Sting$^{gt/gt}$ mice, Rolf Brekken (UTSW) for Tbk1$^{-/-}$ mice, Michael White (UTSW) for Compound II, Shizuo Akira (Osaka U) for the MRX-ibsr retroviral vector; James Koch for technical assistance; experimental support from Washington University Protein Production and Purification Core Facility of the Rheumatic Disease Core Center, members of the Yan lab, Lehrman lab and Morse lab for discussions. Supported by the Rita C. and William P. Clements, Jr. Endowed Scholar Award from UT Southwestern to N.Y., The John P. Perkins, Ph.D. Distinguished Professorship in Biomedical Science from UT Southwestern to M.A.L., the US National Institute of Health (AI098569, AR067135 to N.Y., GM038545 to M.A.L., AR048335 to J.P.A.), Alliance for Lupus Foundation (N.Y.), Welch Foundation (N.Y.), NSF graduate student fellowship (C.F.), private donations from Cure CRV Research, Energy 4 A Cure Foundation and the Robert G. Clark family and Clayco Corporation (J.P.A.) and in part by the Intramural Research Program of the NIH, National Institute of Allergy and Infectious Diseases.

References

Bennett DC, Charest J, Sebolt K, Lehrman M, Rehemtulla A, Contessa JN. High-throughput screening identifies aclacinomycin as a radiosensitizer of EGFR-mutant non-small cell lung cancer. Translational oncology. 2013; 6:382–391. [PubMed: 23730419]

Bodnar RJ, Yates CC, Rodgers ME, Du X, Wells A. IP-10 induces dissociation of newly formed blood vessels. J Cell Sci. 2009; 122:2064–2077. [PubMed: 19470579]

Chui D, Sellakumar G, Green R, Sutton-Smith M, McQuistan T, Marek K, Morris H, Dell A, Marth J. Genetic remodeling of protein glycosylation in vivo induces autoimmune disease. Proc Natl Acad Sci USA. 2001; 98:1142–1147. [PubMed: 11158608]

Cline A, Gao N, Flanagan-Steet H, Sharma V, Rosa S, Sonon R, Azadi P, Sadler KC, Freeze HH, Lehrman MA, Steet R. A Zebrafish Model Of PMM2-CDG Reveals Altered Neurogenesis And A Substrate-Accumulation Mechanism For N-Linked Glycosylation Deficiency. Mol Biol Cell. 2012; 23:4175–4187. [PubMed: 22956764]

Crow YJ, Rehwinkel J. Aicardi-Goutieres syndrome and related phenotypes: linking nucleic acid metabolism with autoimmunity. Hum Mol Genet. 2009; 18:R130–136. [PubMed: 19808788]

Das SC, Nayak D, Zhou Y, Pattnaik AK. Visualization of intracellular transport of vesicular stomatitis virus nucleocapsids in living cells. Journal of virology. 2006; 80:6368–6377. [PubMed: 16775325]

de Silva U, Choudhury S, Bailey SL, Harvey S, Perrino FW, Hollis T. The crystal structure of TREX1 explains the 3′ nucleotide specificity and reveals a polyproline II helix for protein partnering. J Biol Chem. 2007; 282:10537–10543. [PubMed: 17293595]

Fye JM, Orebaugh CD, Coffin SR, Hollis T, Perrino FW. TREX1 dominant mutations in lupus and Aicardi-Goutieres syndrome. J Biol Chem. 2011

Gall A, Treuting P, Elkon KB, Loo YM, Gale M, Barber GN, Stetson DB. Autoimmunity Initiates in Nonhematopoietic Cells and Progresses via Lymphocytes in an Interferon-Dependent Autoimmune Disease. Immunity. 2012; 36:120–131. [PubMed: 22284419]

Gao N, Lehrman MA. Non-radioactive analysis of lipid-linked oligosaccharide compositions by fluorophore-assisted carbohydrate electrophoresis. Methods in enzymology. 2006; 415:3–20. [PubMed: 17116464]

Gao N, Shang J, Huynh D, Manthati VL, Arias C, Harding HP, Kaufman RJ, Mohr I, Ron D, Falck JR, Lehrman MA. Mannose-6-phosphate regulates destruction of lipid-linked oligosaccharides. Mol Biol Cell. 2011; 22:2994–3009. [PubMed: 21737679]

Gehrke N, Mertens C, Zillinger T, Wenzel J, Bald T, Zahn S, Tüting T, Hartmann G, Barchet W. Oxidative damage of DNA confers resistance to cytosolic nuclease TREX1 degradation and potentiates STING-dependent immune sensing. Immunity. 2013; 39:482–495. [PubMed: 23993650]

Green RS, Stone EL, Tenno M, Lehtonen E, Farquhar MG, Marth JD. Mammalian N-glycan branching protects against innate immune self-recognition and inflammation in autoimmune disease pathogenesis. Immunity. 2007; 27:308–320. [PubMed: 17681821]

Grieves JL, Fye JM, Harvey S, Grayson JM, Hollis T, Perrino FW. Exonuclease TREX1 degrades double-stranded DNA to prevent spontaneous lupus-like inflammatory disease. Proceedings of the National Academy of Sciences of the United States of America. 2015

Hasan M, Koch J, Rakheja D, Pattnaik AK, Brugarolas J, Dozmorov I, Levine B, Wakeland EK, Lee-Kirsch MA, Yan N. Trex1 regulates lysosomal biogenesis and interferon-independent activation of antiviral genes. Nat Immunol. 2013; 14:61–71. [PubMed: 23160154]

Holm CK, Paludan SR, Fitzgerald KA. DNA recognition in immunity and disease. Current opinion in immunology. 2013

Kawasaki T, Takemura N, Standley DM, Akira S, Kawai T. The second messenger phosphatidylinositol-5-phosphate facilitates antiviral innate immune signaling. Cell host & microbe. 2013; 14:148–158. [PubMed: 23954154]

Kelleher DJ, Gilmore R. An evolving view of the eukaryotic oligosaccharyltransferase. Glycobiology. 2006; 16:47R–62R.

Lee-Kirsch MA, Gong M, Chowdhury D, Senenko L, Engel K, Lee YA, de Silva U, Bailey SL, Witte T, Vyse TJ, et al. Mutations in the gene encoding the 3′-5′ DNA exonuclease TREX1 are associated with systemic lupus erythematosus. Nat Genet. 2007; 39:1065–1067. [PubMed: 17660818]

Lehtinen DA, Harvey S, Mulcahy MJ, Hollis T, Perrino FW. The TREX1 double-stranded DNA degradation activity is defective in dominant mutations associated with autoimmune disease. J Biol Chem. 2008; 283:31649–31656. [PubMed: 18805785]

Lindahl T, Barnes DE, Yang YG, Robins P. Biochemical properties of mammalian TREX1 and its association with DNA replication and inherited inflammatory disease. Biochemical Society transactions. 2009; 37:535–538. [PubMed: 19442247]

Majima H, Ohta K. Clinical studies of aclacinomycin A (ACM). Biomedicine & Pharmacotherapy. 1987; 41:233–237. [PubMed: 3311189]

Morin MJ, Sartorelli AC. Inhibition of glycoprotein biosynthesis by the inducers of HL-60 cell differentiation, aclacinomycin A and marcellomycin. Cancer research. 1984; 44:2807–2812. [PubMed: 6327026]

Morita M, Stamp G, Robins P, Dulic A, Rosewell I, Hrivnak G, Daly G, Lindahl T, Barnes D. Gene-targeted mice lacking the Trex1 (DNase III) 3′-->5′ DNA exonuclease develop inflammatory myocarditis. Mol Cell Biol. 2004; 24:6719–6727. [PubMed: 15254239]

Richards A, van den Maagdenberg AMJM, Jen JC, Kavanagh D, Bertram P, Spitzer D, Liszewski MK, Barilla-Labarca ML, Terwindt GM, Kasai Y, et al. C-terminal truncations in human 3′-5′ DNA exonuclease TREX1 cause autosomal dominant retinal vasculopathy with cerebral leukodystrophy. Nat Genet. 2007; 39:1068–1070. [PubMed: 17660820]

Saitoh T, Fujita N, Hayashi T, Takahara K, Satoh T, Lee H, Matsunaga K, Kageyama S, Omori H, Noda T, et al. Atg9a controls dsDNA-driven dynamic translocation of STING and the innate immune response. Proc Natl Acad Sci USA. 2009; 106:20842–20846. [PubMed: 19926846]

Stetson DB, Ko JS, Heidmann T, Medzhitov R. Trex1 prevents cell-intrinsic initiation of autoimmunity. Cell. 2008; 134:587–598. [PubMed: 18724932]

Taylor KL, Leaman DW, Grane R, Mechti N, Borden EC, Lindner DJ. Identification of interferon-beta-stimulated genes that inhibit angiogenesis in vitro. Journal of interferon & cytokine research: the official journal of the International Society for Interferon and Cytokine Research. 2008; 28:733–740.

Yan N, Regalado-Magdos AD, Stiggelbout B, Lee-Kirsch MA, Lieberman J. The cytosolic exonuclease TREX1 inhibits the innate immune response to human immunodeficiency virus type 1. Nat Immunol. 2010; 11:1005–1013. [PubMed: 20871604]

Yang Y, Lindahl T, Barnes D. Trex1 Exonuclease Degrades ssDNA to Prevent Chronic Checkpoint Activation and Autoimmune Disease. Cell. 2007; 131:873–886. [PubMed: 18045533]

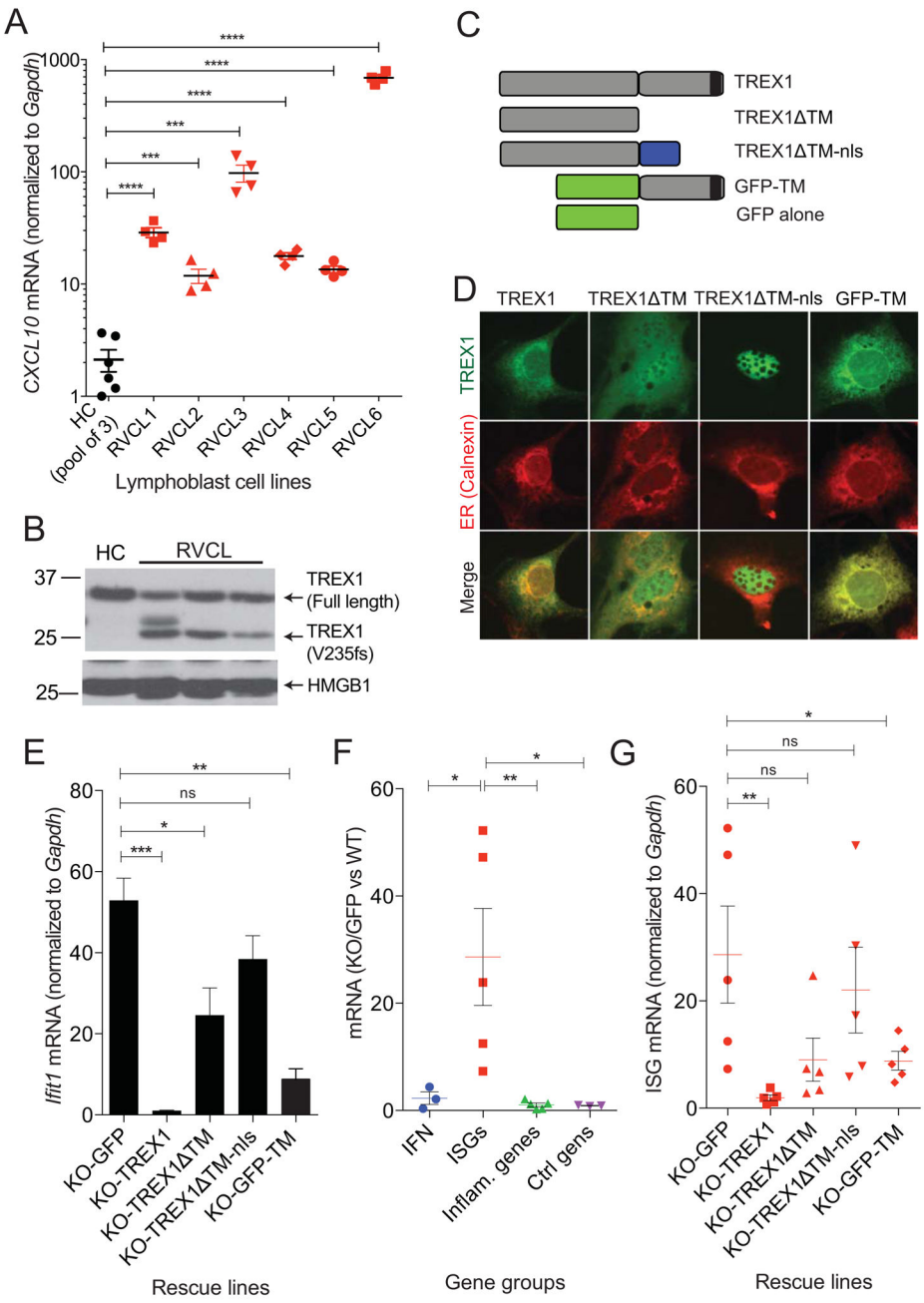

Figure 1. TREX1 C-terminus plays a critical role in suppressing immune activation

(**A**) Quantitative RT-PCR analysis of Cxcl10 mRNA (an ISG) in lymphoblasts from TREX1 patients and healthy controls. Three healthy controls (pooled in 'HC') and six RVCL patients (V235fs) are shown. (**B**) Immunoblot analysis of full length and C terminal truncated TREX1 in control and patient cells. HMGB1 is used as a loading control. (**C**) Diagrams of human TREX1 rescue constructs used in **D–H** and how the rescue lines are generated. (**D**) Fluorescent microscopy of the TREX1 constructs. Trex1$^{-/-}$ MEFs reconstituted with the indicated rescuing construct were fixed and stained with an anti-FLAG antibody (green) or unstained (GFP-TM) and an ER marker anti-Calnexin (red). (**E**)

Quantitative RT-PCR analysis of Ifit1 mRNA (an ISG) in the indicated $Trex1^{-/-}$ rescue MEFs. Gene expression value was normalized to the housekeeping gene, Gapdh. (**F, G**) Quantitative RT-PCR analysis of indicated gene groups in $Trex1^{-/-}$ rescue MEFs. Panel **F** shows KO-GFP cells comparing to WT cells to demonstrate the ISG signature caused by $Trex1^{-/-}$ as shown previously(Hasan et al., 2013). The 'IFN' group contains Ifnb1, Ifna4, Ifng; the 'ISG' group contains Cxcl10, Ifit1, Oasl2, Isg15, Irf7; the 'Inflammatory gene' group contains Il6, Il17a, Tnf, Ccl3, Il23a; and the 'Control gene' group contains Hprt, Gapdh, Actb. Each data point represents one gene. Gene expression values were normalized to the housekeeping gene, Gapdh. Fold increase was then determined by normalizing to WT to aid group signature analysis. Panel **G** shows $Trex1^{-/-}$ rescue cells. Only the ISG group genes are shown. No difference was found in other gene groups. To aid comparison, the same KO-GFP ISG data set is presented in **F** and **G**. *P < 0.05, **P < 0.01, ***P < 0.001, ns = not significant (same throughout). Data are representative of at least three independent experiments. Error bars, SEM (same throughout). Unpaired t-test (A, E). Mann-Whitney test (F, G). See also Figure S1.

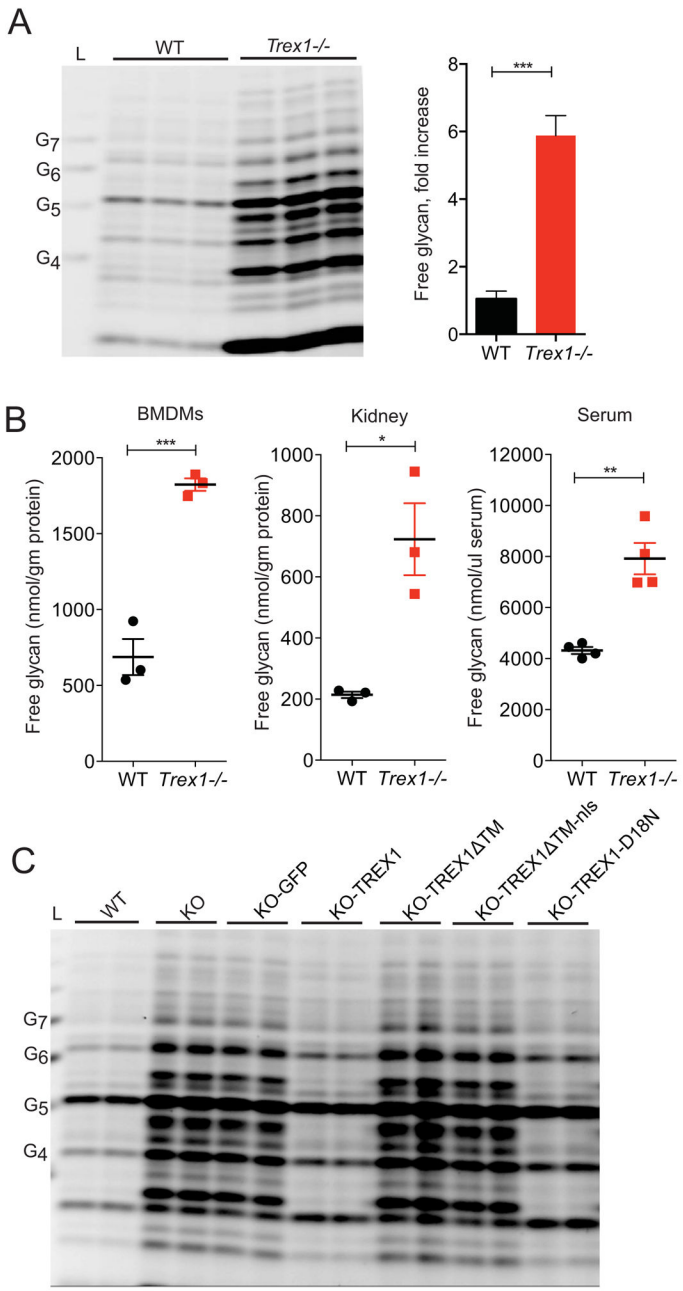

Figure 2. TREX1 C-terminus regulates hydrolysis of lipid-linked oligosaccharides

(**A**) FACE analysis of vesicular free glycans from SLO-permeabilized WT and Trex1$^{-/-}$ MEFs. Similar results were seen with whole cells. L, glucose oligomer glycan ladder (same throughout). Quantification shown in the bar graph on the right. WT normalized to 1. (**B**) Quantification of total free glycans from WT and Trex1$^{-/-}$ mouse BMDMs, kidneys and serum. FACE gels are shown in Figure S2. Each data point is the average value from one individual mouse. (**C**) FACE analysis of total free glycans from WT and Trex1$^{-/-}$ MEFs reconstituted with the indicated rescuing construct. Data are representative of at least three independent experiments. Unpaired t-test (A, B). See also Figure S2.

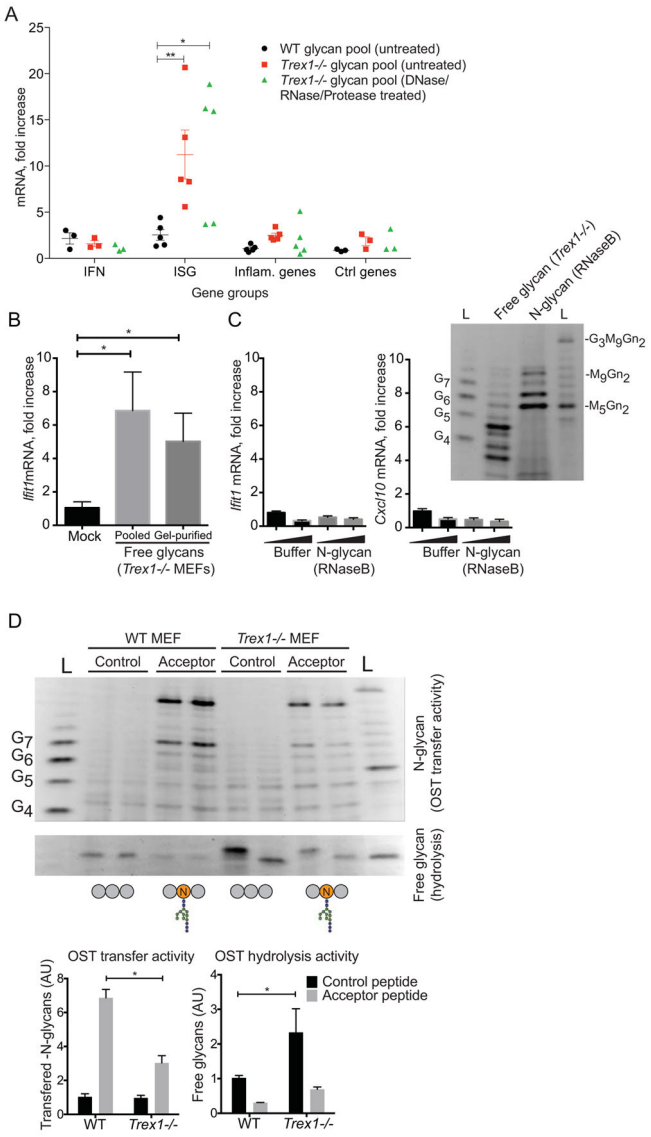

Figure 3. Immunological and biochemical consequences of OST dysregulation

(**A**) Quantitative RT-PCR array analysis of immune gene activation in wild type BMDMs treated with indicated glycans. Free glycans from WT and Trex1$^{-/-}$ MEFs were untreated or treated with a cocktail of DNase, RNase and protease before being added to BMDMs for 20 h. Each data point represents one gene as in Figure 1F. (**B–C**) Quantitative RT-PCR analysis of immune gene activation in wild type BMDMs treated with indicated glycans. Glycan source in **B** is free glycans isolated from Trex1$^{-/-}$ MEFs (pooled glycans) or from FACE gels (gel-purified glycans). Glycan source in **C** is N-glycan isolated from increasing amount of RNase B protein (Sigma Cat#R1153, PNGase digest) or from buffer alone. Ifit1 and Cxcl10 mRNA were analyzed by qRT-PCR. Right, FACE analysis of glycans used in B and C. (**D**) 'In-cell' N-glycosylation assay. WT and Trex1$^{-/-}$ MEFs were permeabilized by SLO and incubated with reaction buffer (see Method) and control or acceptor peptide. Only the acceptor peptide contains one N-glycysolation site. Transferred N-glycans were then cleaved by PNGase and analyzed by FACE (top gel). Free glycans were also analyzed from the same

experiment (bottom gel). Free glycans quantified in this assay are from LLO hydrolysis during the assay, not the pre-existing free glycans in the cell (much smaller in size). Data are representative of at least two independent experiments. Error bars, SEM (same throughout). Mann-Whitney test (A). Unpaired t-test (B). See also Figure S3.

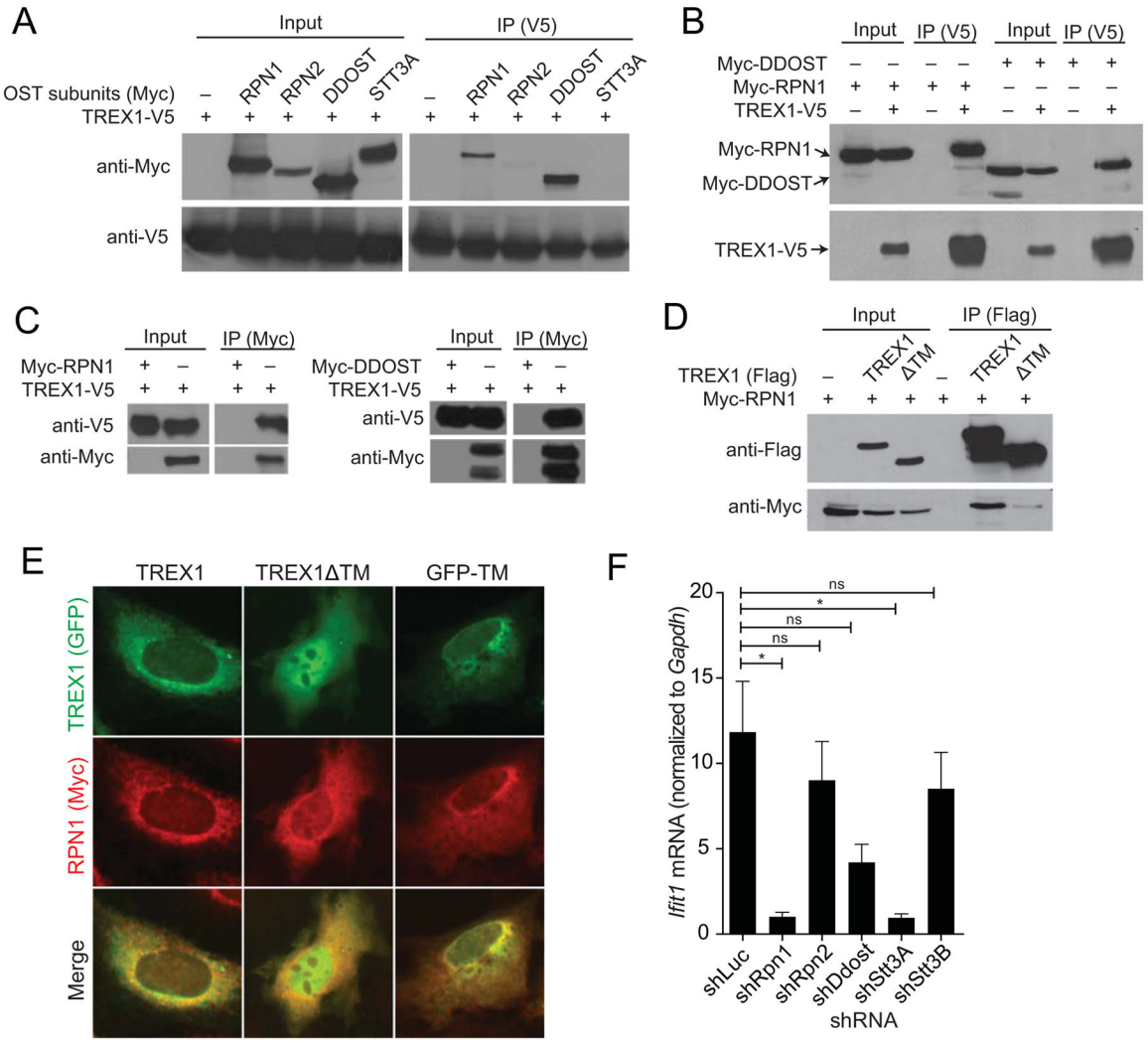

Figure 4. TREX1 interacts with the OST complex through the C-terminus

(**A, B**) Immunoblot analyses of TREX1 interaction with subunits of the OST complex. 293T cells were co-transfected with TREX1-V5 and one subunit of the OST complex as indicated (all Myc-tagged). Immunoprecipitation (IP) was performed with anti-V5 antibody, and precipitated immune complexes were analyzed by immunoblot with anti-V5 antibody (to detect primary IP of TREX1) and anti-Myc (to detect co-IP of individual OST subunits). The absolute requirement for TREX1 is emphasized in **B**. (**C**) Immunoblot analysis of TREX1 interactions with RPN1 and DDOST. 293T cells were transfected with plasmids indicated on top. Immunoprecipitation (IP) was performed with anti-Myc antibody. **(D)** The TREX1 C-terminus is required for interaction with RPN1. 293T cells were co-transfected with Myc-RPN1 and the indicated TREX1 (Flag-tagged) plasmids on top. Co-IP was performed with anti-Flag antibody. (**E**) Immunofluorescent microscopy analyses of TREX1 and RPN1 colocalization. GFP-TREX1, GFP-TREX1_TM or GFP-TM were co-transfected with Myc-RPN1, and immunostained with anti-Myc (red) 24 h later. (**F**) Rpn1 and Stt3a are required for immune activation in Trex1$^{-/-}$ cells. Trex1$^{-/-}$ MEFs were transduced with lentiviruses expressing specific shRNAs as indicated. Expression of Ifit1 mRNA was

measured by RT-qPCR. Specific knockdown of individual genes was verified by RT-qPCR in Figure S4. Data are representative of at least three independent experiments. Unpaired t-test (F). See also Figure S4.

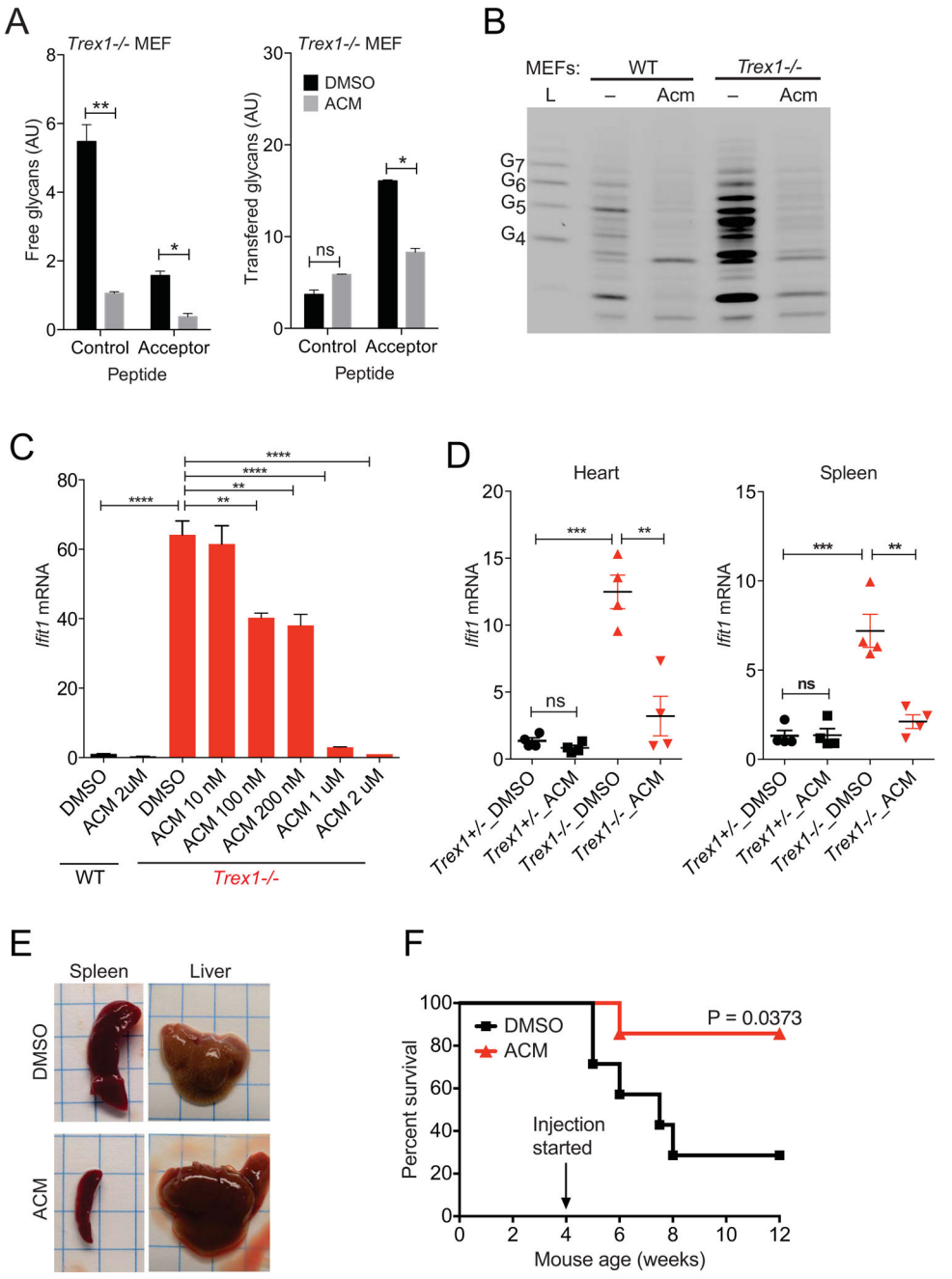

Figure 5. Inhibiting OST activity by aclacinomycin (Acm) suppresses free glycan release, immune activation and disease in *Trex1*$^{-/-}$ mice

(**A**) Acm inhibits both OST activities in Trex1$^{-/-}$ cells. Representative images of FACE gels are shown in Figure S5. (**B, C**) FACE analysis of free glycans (**B**) and quantitative RT-PCR analysis of immune gene activation (**C**) or in WT and Trex1$^{-/-}$ MEFs treated with Acm. WT and Trex1$^{-/-}$ MEFs were treated with increasing concentration of Acm or DMSO for 24 h. Ifit1 mRNA were measured by qPCR. Cells treated with 2 micromolar Acm were used for free glycan analysis in **C**. (**D–F**) In vivo treatment with Acm. Trex1$^{+/-}$ and Trex1$^{-/-}$ mice were treated with DMSO or Acm (5 mg/kg) for 8 weeks. Quantitative RT-PCR analysis of

Ifit1 mRNA in mouse heart and spleen after 1 week of treatment are shown in **D** (n=4). Representative images of spleen and liver are shown in **E**. Survival curve after 8-week of treatment is shown in **F** (n=7). Unpaired t-test (A, C, D). Logrank test (F). See also Figure S5.

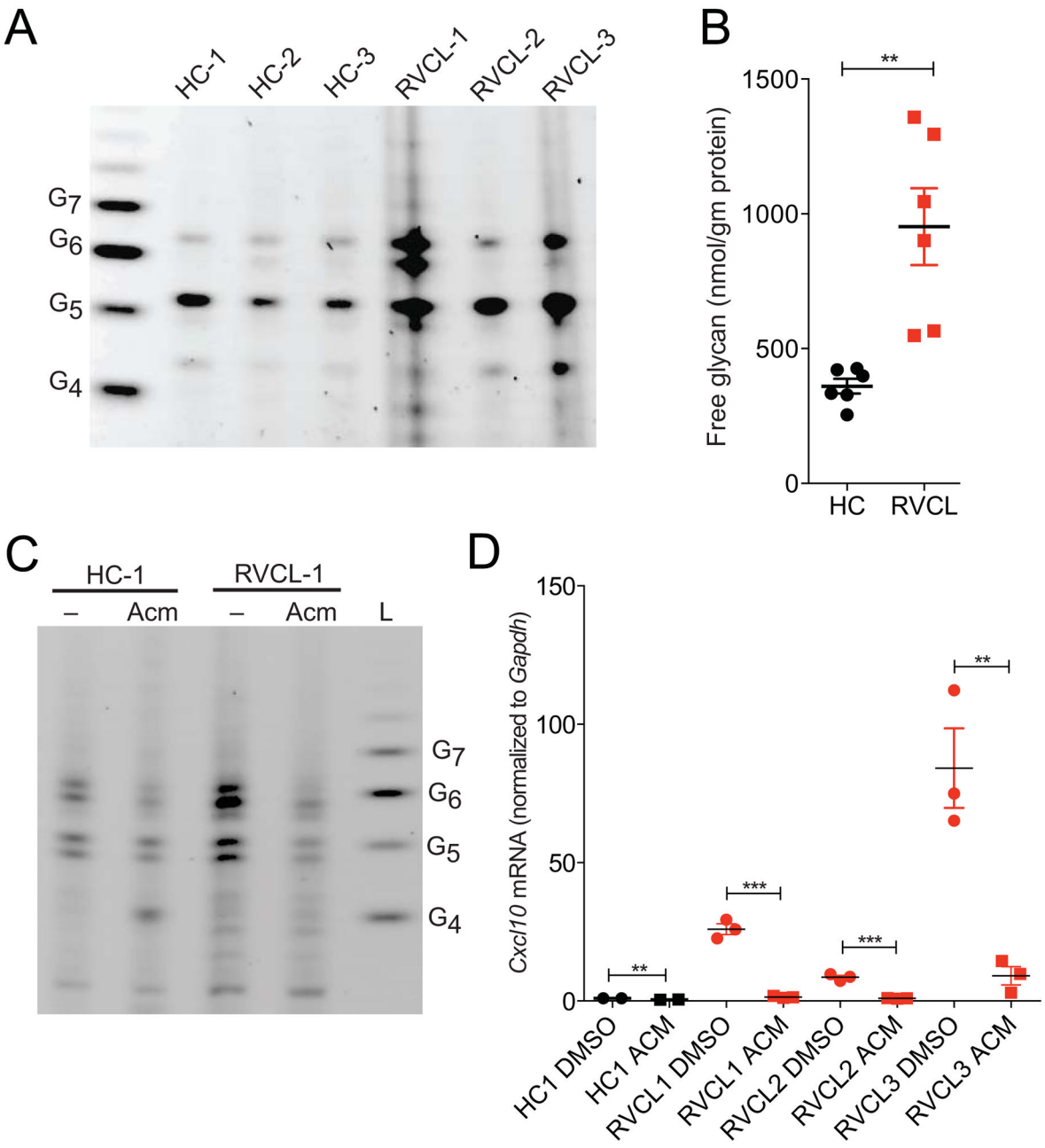

Figure 6. TREX1 RVCL patient lymphoblasts show elevated free glycans and immune gene expression

(**A, B**) FACE analysis of free glycans in lymphoblasts from RVCL patients and healthy controls. Three healthy controls, three RVCL patients (V235fs) are shown individually in **A**. Duplicate measurements of total free glycans in each individual are shown in **B**. (**C**, **D**) Free glycan and ISG analysis of lymphoblasts from RVCL patients and healthy controls treated with 1 micromolar Acm for 24 hrs. Data are representative of at least three independent experiments. Unpaired t-test (B, D).

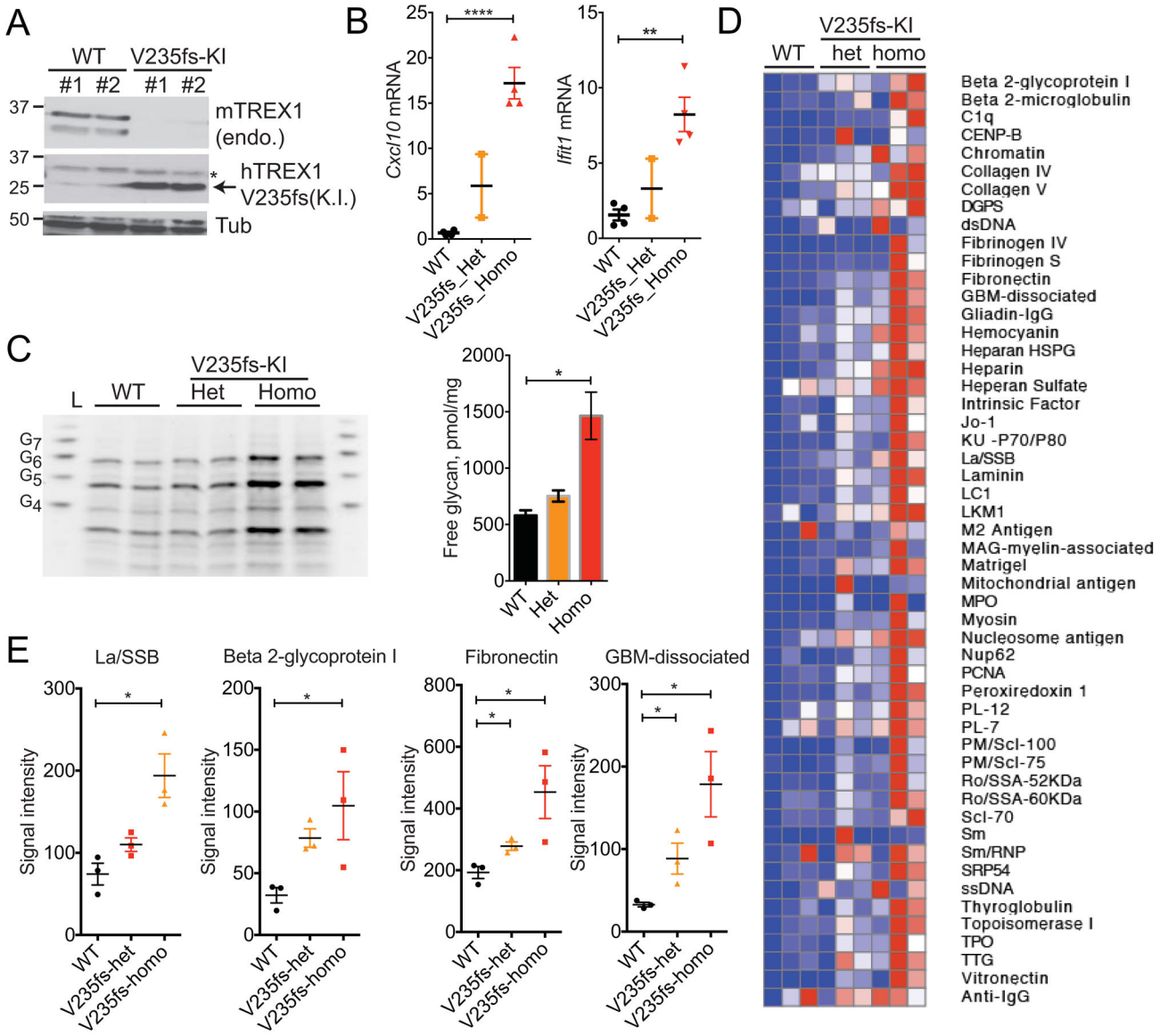

Figure 7. TREX1-V235fs knock-in (KI) mouse display elevated free glycan, ISG signature and autoantibodies

(**A**) Immunoblot analysis of TREX1 in BMDMs isolated from two independent WT or V235fs-KI homozygous mice. (**B**) Quantitative RT-PCR analysis of ISGs in BMDMs of indicated genotype. (**C**) FACE analysis of free glycans in BMDMs of indicated genotype. (**D, E**) Autoantibody array analysis of serum isolated from WT, V235fs heterozygous or homozygous mice (8-month old). Representative autoantibodies are shown in **E**. n=3. Data are representative of at least two independent experiments. Unpaired t-test (B, C, E). See also Figure S6.